Synthesis, Crystal Structures and Properties of Three New Tetrathiomolybdates with Organic Ammonium Cations

Bikshandarkoil R. Srinivasan[a], Sunder N. Dhuri[a], Martha Poisot, Christian Näther, and Wolfgang Bensch

Institut für Anorganische Chemie, Christian-Albrechts-Universität Kiel, Olshausenstraße 40, D-24098 Kiel, Germany
[a] Department of Chemistry, Goa University PO, Goa 403 206, India

Reprint requests to Prof. Dr. Wolfgang Bensch. Fax: +49-(0)431-880-1520.
E-mail: wbensch@ac.uni-kiel.de

Z. Naturforsch. **59b,** 1083 – 1092 (2004); received June 9, 2004

Dedicated to Prof. Dr. Wilhelm Preetz on the occasion of his 70th birthday

Three new tetrathiomolybdates $(pipH_2)[MoS_4]$ (**1**), $(trenH_2)[MoS_4]\cdot H_2O$ (**2**) and $[(prop)_4N]_2[MoS_4]$ (**3**) (pip = piperazine, tren = tris(2-aminoethyl)amine and prop = *n*-propyl) were synthesized and characterized by elemental analysis, infrared spectroscopy, single crystal X-ray crystallography, and thermoanalysis. All compounds were prepared by the base promoted cation exchange method, *i.e.* by the reaction of the ammonium salt of $[MoS_4]^{2-}$ with the corresponding organic amine or organic ammonium hydroxide. In the compounds **1** and **2** the organic amines pip and tren are diprotonated and they are linked to the tetrahedral $[MoS_4]^{2-}$ dianions through weak hydrogen bonding interactions. The strength and number of these hydrogen bonds affect the Mo-S bond lengths and a relatively long Mo-S bond of 2.2114(8) Å is observed in **1** while the longest Mo-S bond in **2** is 2.1951(5) Å. In compound **3** no S···H-N interactions are possible and the Mo-S bond lengths scatter in a more narrow range compared to those in compounds **1** and **2**. The thermal behavior was investigated using differential thermal analysis and thermogravimetry. On heating compound **1** decomposes in two closely related steps while **2** loses first the crystal water followed by the decomposition of the tetrathiomolybdate. The final products are amorphous molybdenum sulfides. The decomposition of compound **3** yields a very porous material with sponge-like morphology.

Key words: Thiomolybdates, Crystal Structures, Thermal Properties, Optical Properties

Introduction

The chemistry of soluble metal sulfide complexes is emerging as a frontier area of research in view of the relevance of metal sulfide compounds in hydrodesulfurization catalysis (HDS), energy, environmental and material science [1]. In recent years, the use of tetraalkylammonium tetrathiomolybdates as precursor materials for the preparation of MoS_2 catalysts is showing much promise in the field of HDS catalysis [2]. The nature of the alkyl group in the precursors has been shown to affect the surface area, pore size distribution as well as HDS selectivity. Current and future investigations will be focused on the preparation of HDS catalysts, which have a large specific surface and a distinct ratio of rim and edge sites. The field of catalytically active transition metal sulfides has been reviewed [3, 4]. The synthesis and HDS activity of Ni-Mo-S catalysts [5] and Co-Mo-S catalysts [6] both derived from thiomolybdates have been reported recently.

The group VI metal Mo exhibits a wide range of metal to sulfur stoichiometries, metal oxidation states, coordination geometries and bonding modes of the sulfido ligands [7]. A variety of structurally diverse Mo-S compounds like $[MoS(S_4)_2]^{2-}$, $[Mo_2(S)_2(\mu\text{-}S)_2(S_2)_2]^{2-}$, $[Mo_2(S)_2(\mu\text{-}S)_2(S_4)(S_2)]^{2-}$, $[Mo_2(S)_2(\mu\text{-}S)_2(S_4)_2]^{2-}$, $[SMo(MoS_4)_2]^{2-}$ *etc.* have been prepared from tetrathiomolybdates by reacting with the appropriate reagents, which indicates the importance of the $[MoS_4]^{2-}$ moiety as a building block for the synthesis of several novel Mo-S complexes [8 – 12]. In recent years the use of tetrathiomolybdate for the treatment of metastatic cancer has added an entire new dimension to its chemistry [13, 14]. Although $[MoS_4]^{2-}$, one of the simplest soluble Mo-S complexes, has been known from the days of Berzelius

[15], a systematic chemistry of this complex has been developed only in the last two to three decades primarily by Müller and coworkers [16]. The use of thiomolybdate as a versatile reagent for the preparation of a variety of compounds and also its relevance in bioinorganic chemistry and medicine has been recently reviewed [17]. It has been shown by Bezverkhyy *et al.* that $[MoS_4]^{2-}$ can be used as a precursor for the facile synthesis of highly dispersed MoS_2 [18]. The same group has reported that the chemical properties of $[MoS_4]^{2-}$ can be substantially changed by surrounding it with organic ammonium cations for example cetyltriethyl ammonium [19]. This report gains further credence from the work of Rauchfuss and co-workers wherein the reactivity characteristics of $[MoS_4]^{2-}$ towards PMe_3 (Me is methyl) have been reported [20]. Here it has been shown that acetonitrile solutions of $(Et_4N)_2[MoS_4]$ (Et is ethyl) and PMe_3 are stable, while acetonitrile solutions of $(NH_4)_2[MoS_4]$ and PMe_3 react to form the hexacoordinated Mo(IV) complex $[MoS_2(PMe_3)_4]$ indicating the role of proton sources for S transfer. A possible reason for this differing reactivity of $(NH_4)_2[MoS_4]$ and$(Et_4N)_2[MoS_4]$ has been attributed to the short H-bonding contacts between the cation and anion in $(NH_4)_2[MoS_4]$ [20], a structural feature which is absent in $(Et_4N)_2[MoS_4]$ [21].

In our work we have shown the importance of hydrogen bonding interactions in the lengthening of M-S (M = Mo or W) bond distances in several $[MS_4]^{2-}$ complexes [22 – 31]. The above observations taken together with our recent results in this area clearly indicate that a rich chemistry of thiomolybdates can be developed by suitably changing the hydrogen bonding interactions between the cation and $[MoS_4]^{2-}$. These studies can then be useful to derive a structure-function correlation in terms of the M-S bond distances. The H-bonding interactions in thiomolybdates can be fine tuned by a proper choice of the amine, which differs in its bulkiness and also the number of potential H-bonding donors attached to the amino nitrogen atoms. In the present work we have employed the cyclic amine piperazine (pip), the polyamine tris(2-aminoethylamine) (tren) and tetra-*n*-propylammonium hydroxide $[(prop)_4N]OH$ generated *in situ* from $[(prop)_4N]Br$ and NaOH, for the cation exchange reaction with ammonium tetrathiomolybdate. From these reactions we have isolated the compounds $(pipH_2)[MoS_4]$ (**1**), $(trenH_2)[MoS_4]\cdot H_2O$ (**2**) and $[(prop)_4N]_2[MoS_4]$ (**3**). In compound **1** both N atoms of pip are protonated resulting in the formation of $(pipH_2)^{2+}$, while only two of the four N atoms are protonated in **2** leading to the formation of $(trenH_2)^{2+}$. The structure of compound **1** which was reported earlier [32] has been redetermined by us at low temperatures, because the quality of the earlier structural data was poor. In compound **3** the N atoms of the cations are fully alkylated and hence S···H-N bonding is not possible. The compounds have been characterized by elemental analysis, infrared spectroscopy, single crystal X-ray crystallography and thermoanalysis. The results of these investigations are described in this paper.

Experimental Section

Materials and methods

The amines pip, tren, tetra-*n*-propylammonium bromide and ammonium heptamolybdate and the solvents were used in this investigation as obtained from commercial sources. $(NH_4)_2[MoS_4]$ was freshly prepared by literature method [33]. Far-IR spectra (range 80 to 500 cm^{-1}) were measured on a Bruker IFS 66 infrared spectrometer in pressed polyethylene disks. MIR spectra of the compounds were recorded in a KBr matrix. The samples were ground with dry KBr into fine powders and pressed into transparent pellets. The spectra were recorded in the IR region of 450 to 3000 cm^{-1}, (resolution 1 cm^{-1}) with a ATI Mattson Genesis infrared spectrometer. Raman spectra were measured in the region from 100 to 3500 cm^{-1} on a Bruker IFS 66 Fourier transform Raman spectrometer. DTA-TG measurements were performed simultaneously using the STA-409CD device (Netzsch). The thermal investigations were performed in Al_2O_3 crucibles using a heating rate of 4 K/min up to 600 °C and purged in a nitrogen stream of approximately 75 ml/min. EDX analysis was performed with a Philips ESEM XL 30 scanning electron microscope equipped with an EDAX analyzer. X-ray powder patterns were recorded in transmission geometry using a STOE STADI P diffractometer (Cu-$K_\alpha = 1.54056$ Å).

*Preparation of $(pipH_2)[MoS_4]$ (**1**)*

Freshly prepared ammonium tetrathiomolybdate (260 mg, 1 mmol) was dissolved in distilled water (15 ml) and anhydrous piperazine (86 mg, 1 mmol) dissolved in distilled water (5 ml) was added at room temperature. The reaction mixture was stirred for ∼ 5 min and then filtered. The clear filtrate was left undisturbed in a refrigerator. After 2 days red blocks of compound **1** were obtained which were filtered, washed with ice-cold water (2 ml) followed by isopropanol (10 ml) and diethylether (10 ml), and dried under vacuum. Yield 65%. – IR data: 3000 (br), 1544, 1440, 1371, 1297, 1186, 1079, 910, 862, 655, 556, 479, 465, 445, 336, 267, 200, 133, and 93 cm^{-1}. – Raman Data: 496, 478, 469, 448, 438,

Table 1. Technical details of data acquisition and selected refinement results for $(pipH_2)[MoS_4]$ **1**, $(trenH_2)[MoS_4]\cdot H_2O$ **2**, and $[(prop)_4N]_2[MoS_4]$ **3**.

Compound	$(pipH_2)$-$[MoS_4]$ (**1**)	$(trenH_2)$-$[MoS_4]\cdot H_2O$ (**2**)	$[(prop)_4N]_2$-$[MoS_4]$ (**3**)
Formula	$C_4H_{12}MoN_2S_4$	$C_6H_{22}N_4OMoS_4$	$C_{24}H_{56}N_2MoS_4$
MW [g/mol]	312.36	390.47	596.93
Space group	$P2_1/c$	$P2_1/c$	$C2/c$
a [Å]	8.2520(9)	11.470(2)	32.334(4)
b [Å]	11.238(1)	11.793(2)	13.812(2)
c [Å]	11.929(2)	12.483(2)	15.017(3)
β [°]	95.20(2)	111.63(1)	109.24(2)
Volume [Å^3]	1101.7(2)	1569.5(4)	6331.7(2)
Z	4	4	8
Temperature / K	293	293	293
μ [mm^{-1}]	1.90	1.356	0.69
$F(000)$	624	800	2560
$d_{calc.}$ [g· cm^{-3}]	1.883	1.652	1.252
2θ Range [°]	3 – 60	3 – 60	3 – 60
hkl Range	0/11; −14/4; −16/16	−16/1; −16/16; −16/17	−42/40; −18/12; 0/19
Refls collected	5058	9614	14726
Refls unique	3217	4588	7657
Data $[F_o>4\sigma(F_o)]$	2258	3990	5001
$R_{int.}$	0.0535	0.0229	0.0395
min./max transm.	–	0.7867 / 0.8513	–
$\delta\rho$ [e/Å^3]	−0.69 /0.670	−0.80 /0.46	0.28 / −0.47
Parameters	101	146	511
R_1 $[F_o>4\sigma(F_o)]$[a]	0.0290	0.0209	0.0305
$wR2$ for all data	0.0730	0.0560	0.0758
Goodness of fit	1.017	1.042	0.977

[a] $R_1 = \Sigma||Fo| - |Fc||/\Sigma|Fo|$.

Table 2. Atomic coordinates [$\times 10^4$] and equivalent isotropic displacement parameters [Å$^2 \times 10^3$] for $(pipH_2)[MoS_4]$ **1**.

Atom	x	y	z	U_{eq}
Mo(1)	7927(1)	2790(1)	5944(1)	22(1)
S(1)	7930(1)	3920(1)	7418(1)	30(1)
S(2)	5739(1)	1646(1)	5854(1)	29(1)
S(3)	10115(1)	1663(1)	6118(1)	29(1)
S(4)	7924(1)	3860(1)	4431(1)	33(1)
N(1)	4594(3)	2698(2)	8239(2)	29(1)
C(1)	3680(3)	1576(3)	8328(2)	29(1)
C(2)	2314(3)	1739(3)	9079(2)	28(1)
N(2)	1242(3)	2737(2)	8668(2)	28(1)
C(3)	2168(4)	3864(3)	8582(3)	34(1)
C(4)	3525(4)	3693(3)	7823(3)	32(1)

U_{eq} is calculated as one third of the trace of the orthogonalised U_{ij} tensor.

199, 184 and 175 cm^{-1}. – Analysis found (calcd): C 15.04 (15.38), H 3.83 (3.88), N 8.71 (8.97), S 40.95 (41.06).

*Preparation of $(trenH_2)[MoS_4]\cdot H_2O$ (**2**)*

Freshly prepared ammonium tetrathiomolybdate (520 mg, 2 mmol) was dissolved in distilled water (50 ml) containing 5 drops of ammonia solution. An aqueous tren solution

Table 3. Atomic coordinates [$\times 10^4$] and equivalent isotropic displacement parameters [Å$^2 \times 10^3$] for $(trenH_2)[MoS_4] \cdot H_2O$ **2**.

Atom	x	y	z	U_{eq}
Mo(1)	1787(1)	3575(1)	2323(1)	26(1)
S(1)	53(1)	3020(1)	2509(1)	41(1)
S(2)	1543(1)	3576(1)	498(1)	35(1)
S(3)	3266(1)	2420(1)	3299(1)	40(1)
S(4)	2250(1)	5303(1)	3001(1)	39(1)
N(1)	6392(1)	3908(1)	3075(1)	29(1)
C(1)	6714(1)	2725(1)	3417(1)	33(1)
C(2)	8024(1)	2645(1)	4327(1)	34(1)
N(2)	8369(1)	1440(1)	4636(1)	34(1)
C(3)	5928(2)	4490(1)	3883(1)	34(1)
C(4)	6272(2)	5731(2)	4004(1)	43(1)
N(3)	7644(2)	5876(1)	4469(1)	46(1)
C(5)	5477(2)	4004(2)	1886(1)	36(1)
C(6)	6023(2)	3710(2)	981(1)	39(1)
N(4)	7069(2)	4412(1)	976(1)	43(1)
O(1)	9395(2)	5453(2)	3441(2)	86(1)

Table 4. Atomic coordinates [$\times 10^4$] and equivalent isotropic displacement parameters [Å$^2 \times 10^3$] for $[(prop)_4N]_2$-$[MoS_4]$ **3**.

Atom	x	y	z	U_{eq}
Mo(1)	3732(1)	7430(1)	4146(1)	36(1)
S(1)	4195(1)	6680(1)	3596(1)	51(1)
S(2)	3165(1)	7934(1)	2983(1)	56(1)
S(3)	3504(1)	6435(1)	5006(1)	61(1)
S(4)	4056(1)	8660(1)	5010(1)	60(1)
N(1)	2550(1)	4890(1)	6034(1)	34(1)
C(1)	2485(1)	5318(2)	5058(1)	35(1)
C(2)	2197(1)	6197(2)	4787(2)	45(1)
C(3)	2179(1)	6536(2)	3813(2)	49(1)
C(4)	2112(1)	4630(2)	6138(2)	42(1)
C(5)	1830(1)	3937(2)	5409(2)	56(1)
C(6)	1418(1)	3706(2)	5627(2)	64(1)
C(7)	2770(1)	5639(2)	6777(1)	41(1)
C(8)	2876(1)	5297(2)	7791(2)	65(1)
C(9)	3095(1)	6085(3)	8459(2)	96(1)
C(10)	2829(1)	3983(2)	6141(2)	42(1)
C(11)	3310(1)	4137(2)	6277(2)	47(1)
C(12)	3515(1)	3196(2)	6119(2)	52(1)
N(2)	5000	9109(2)	2500	36(1)
C(21)	5070(1)	8454(2)	3351(2)	40(1)
C(22)	5116(1)	8970(2)	4275(2)	53(1)
C(23)	5205(1)	8250(2)	5075(2)	58(1)
C(24)	5397(1)	9758(2)	2640(2)	44(1)
C(25)	5823(1)	9242(2)	2777(2)	58(1)
C(26)	6180(1)	9970(2)	2792(2)	75(1)
N(3)	5000	4220(2)	2500	44(1)
C(31)	5224(2)	5056(5)	3192(4)	53(1)
C(32)	5424(2)	4808(5)	4222(4)	72(2)
C(31')	5124(2)	4575(4)	3469(4)	47(1)
C(32')	5486(2)	5321(5)	3731(5)	63(2)
C(33)	5594(1)	5632(2)	4786(2)	83(1)
C(34)	5338(2)	3395(4)	2648(4)	48(1)
C(35)	5771(2)	3621(5)	2500(4)	64(2)
C(34')	5366(2)	3842(4)	2179(4)	56(1)
C(35')	5606(2)	3028(5)	2733(5)	73(2)
C(36)	6025(1)	2754(3)	2540(2)	95(1)

Table 5. Selected interatomic distances (Å) and angles (°) for $(pipH_2)[MoS_4]$ **1**, $(trenH_2)[MoS_4]\cdot H_2O$ **2** and $[(prop)_4N]_2[MoS_4]$ **3**.

$(pipH_2)[MoS_4]$ **1**:			
Mo(1)–S(4)	2.1683(8)	Mo(1)–S(1)	2.1687(8)
Mo(1)–S(3)	2.2004(7)	Mo(1)–S(2)	2.2114(8)
S(4)–Mo(1)–S(1)	110.48(3)	S(4)–Mo(1)–S(3)	109.71(3)
S(1)–Mo(1)–S(3)	108.66(3)	S(4)–Mo(1)–S(2)	110.04(3)
S(1)–Mo(1)–S(2)	108.71(3)	S(3)–Mo(1)–S(2)	109.21(3)
$(trenH_2)[MoS_4]\cdot H_2O$ **2**:			
Mo(1)–S(3)	2.1670(5)	Mo(1)–S(1)	2.1856(5)
Mo(1)–S(2)	2.1905(5)	Mo(1)–S(4)	2.1951(5)
S(3)–Mo(1)–S(1)	107.89(2)	S(3)–Mo(1)–S(2)	110.97(2)
S(1)–Mo(1)–S(2)	109.79(2)	S(3)–Mo(1)–S(4)	109.79(2)
S(1)–Mo(1)–S(4)	109.71(2)	S(2)–Mo(1)–S(4)	108.68(2)
$[(prop)_4N]_2[MoS_4]$ **3**:			
Mo(1)–S(3)	2.1749(7)	Mo(1)–S(4)	2.1837(7)
Mo(1)–S(2)	2.1885(8)	Mo(1)–S(1)	2.1928(7)
S(3)–Mo(1)–S(4)	109.19(3)	S(3)–Mo(1)–S(2)	108.34(3)
S(4)–Mo(1)–S(2)	109.76(3)	S(3)–Mo(1)–S(1)	109.48(3)
S(4)–Mo(1)–S(1)	109.79(3)	S(2)–Mo(1)–S(1)	110.25(3)

(0.5 ml in 10 ml water) was added at room temperature. The reaction mixture was filtered and the clear filtrate was left undisturbed. After a day red blocks of compound **2** were obtained, which were filtered, washed with ice-cold water (2 ml), followed by isopropanol (15 ml) and diethylether (20 ml), and dried under vacuum. Yield 70%. – IR data: 3462 (br), 3328(w), 3277(w), 3072, 3004, 2924, 2829, 1601, 1569, 1513, 1464, 1345, 1295, 1115, 1071, 1007, 963, 857, 755, 487, 467, 450, 357, 344, 248, 215, 203, 185, 132, and 101 cm^{-1}. – Analysis found (calcd): C 18.34 (18.45), H 5.71 (5.64), N 14.23 (14.35), S 32.63 (32.85).

*Preparation of $[(prop)_4N]_2[MoS_4]$ (**3**)*

Freshly prepared $(NH_4)_2MoS_4$ (2 g, 7.7 mmol) was dissolved in distilled water (60 ml). This solution was added to a mixture of tetra-*n*-propylammonium bromide (4 g, 15.4 mmol) and NaOH (0.6 g, 15.5 mmol) in distilled water (10 ml). The resulting solution was stirred at room temperature for 10 min and then kept undisturbed overnight, precipitating red crystals of $[(prop)_4N]_2MoS_4$. The crystalline compound was filtered, washed with ice-cold water (2 ml), followed by isopropanol (15 ml) and diethylether (20 ml), and dried under vacuum. Yield 80%. – IR data: 2965 (br), 2931, 2871, 1470 (s), 1376 (w), 1325 (w), 970 (s), 759 (w), 475 (sh), 465 (s), 448 (w), cm^{-1}. – Analysis found (calcd): C 47.95 (48.3), H 9.5 (9.4), N 4.6 (4.7), S 20.8 (21.5).

Single crystal X-ray diffractometry

Intensity data for compounds **1**–**3** were collected on a AED2 four circle diffractometer at room temperature using graphite monochromated Mo-K_α radiation. For **2** a numerical absorption correction was applied. All structures were solved with direct methods using SHELXS-97 [34] and refinement was carried out against F^2 using SHELXL-97 [35]. All non-hydrogen atoms were refined using anisotropic displacement parameters. The hydrogen atoms were positioned with idealized geometry and refined using the riding model with fixed isotropic displacement parameters. Four carbon atoms of one of the three crystallographically independent tetra-*n*-propylammonium cations were disordered in two positions and were refined using a split model. The technical details of data acquisition and some selected refinement results are summarized in Table 1. The atomic coordinates and equivalent isotropic displacement parameters for compounds **1**–**3** are presented in Tables 2–4. Selected bond lengths, and bond angles for compounds **1** to **3** and hydrogen bonding parameters are listed in Tables 5–7.

Table 6. Hydrogen-bonding geometry (Å, °) for $(pipH_2)[MoS_4]$ **1**.

D-H···A	d(D-H)	d(H···A)	d(D···A)	∠DHA	Symmetry code
N1-H1A···S2	0.900	2.561	3.298	139.62	
N1-H1A···S1	0.900	2.648	3.303	130.33	
N1-H1B···S2	0.900	2.379	3.260	166.21	$x, -y+\frac{1}{2}, z+\frac{1}{2}$
N2-H2C···S3	0.900	2.465	3.219	141.50	$x-1, -y+\frac{1}{2}, z+\frac{1}{2}$
N2-H2C···S4	0.900	2.884	3.465	123.65	$x-1, -y+\frac{1}{2}, z+\frac{1}{2}$
N2-H2D···S3	0.900	2.454	3.255	162.91	$x-1, y, z$
N2-H2D···S1	0.900	2.819	3.274	112.72	$x-1, y, z$

Table 7. Hydrogen-bonding geometry (Å, °) for $(trenH_2)[MoS_4]\cdot H_2O$ **2**.

D-H…A	d D-H	d H…A	d D…A	∠ DHA	Symmetry code
N1-H1···S2	0.860	2.583	3.396	158.03	$x+1, -y+\frac{1}{2}, z+\frac{1}{2}$
N1-H1···S1	0.860	2.936	3.448	120.06	$x+1, -y+\frac{1}{2}, z+\frac{1}{2}$
N2-H2···S4	0.860	2.530	3.379	169.34	$-x+1, y-\frac{1}{2}, -z+\frac{1}{2}$
N2-H2···S2	0.860	2.992	3.386	110.12	$-x+1, y-\frac{1}{2}, -z+\frac{1}{2}$
N2-H3···N4	0.860	1.946	2.805	177.06	$x, -y+\frac{1}{2}, z+\frac{1}{2}$
N3-H1···S4	0.860	2.623	3.413	153.12	$-x+1, -y+1, -z+1$
N3-H2···O1	0.860	1.985	2.797	157.11	
N3-H3···S2	0.860	2.458	3.313	172.51	$-x+1, y+\frac{1}{2}, -z+\frac{1}{2}$
N4-H1···S3	0.890	2.929	3.715	148.18	$-x+1, y+\frac{1}{2}, -z+\frac{1}{2}$
N4-H2···S1	0.890	3.019	3.638	128.29	$x+1, y, z$
O1-H1···S1	0.820	2.499	3.286	161.38	$x+1, y, z$
O1-H2···S1	0.820	2.586	3.395	169.33	$-x+1, y+\frac{1}{2}, -z+\frac{1}{2}$

Crystallographic data (excluding structure factors) have been deposited with the Cambridge Crystallographic Data Centre as supplementary publication no. CCDC 241130 (**1**), CCDC 241131 (**2**) and CCDC 241132 (**3**). Copies of the data can be obtained, free of charge, on application to CCDC, 12 Union Road, Cambridge CB2 1 EZ, UK. (fax: +44-(0)1223-336033 or email: deposit@ccdc.cam.ac.uk).

Results and Discussion

Synthetic aspects

The synthesis of the title compounds has been readily accomplished in good yields by reacting $(NH_4)_2[MoS_4]$ with the corresponding organic amines. In the synthesis of **3**, tetra-*n*-propylammonium hydroxide is generated *in situ* by the reaction of tetra-n-propylammonium bromide with NaOH, which then functions as the organic base. The formation of the title complexes from ammonium tetrathiomolybdate on treatment with the organic amines can be explained as a base promoted cation exchange reaction, wherein the stronger organic base replaces the weak ammonia of $(NH_4)_2[MoS_4]$ as shown below. We have used a similar methodology for the isolation of tetrathiomolybdates as well as tetrathiotungstates $[MS_4]^{2-}$ (M = Mo, W) with ethylenediammonium, 1,3-propanediammonium, N,N,N',N'-tetramethylethylenediammonium and 1,4-dimethylpiperazinium cations indicating the generality of this reaction [26 – 30].

$$(NH_4)_2[MoS_4] + \textit{amine/ammoniumhydroxide} \rightarrow \mathbf{1} - \mathbf{3} + 2\,NH_3$$

The compounds are quite stable in air and less soluble in water unlike ammonium tetrathiomolybdate.

Crystal structures

In the structures of the title compounds tetrahedral $[MoS_4]^{2-}$ anions and the counter cations $(pipH_2)^{2+}$ (in **1**), $(trenH_2)^{2+}$ (in **2**), and $[(prop)_4N]^+$ (in **3**) are found. In **1** and **2** all unique atoms are on general positions whereas in **3** N(2) and N(3) are located on special positions. In compound **1** piperazinium cations and tetrahedral $[MoS_4]^{2-}$ anions are connected *via* weak hydrogen bonds. In **1** the cyclic organic cation adopts the chair form and the C-C and C-N bond lengths and bond angles are in good agreement with those reported for other complexes containing the same cation [36,37]. The MoS_4 tetrahedron is distorted with S-Mo-S angles between 108.66(3) and 110.04(3)°. The Mo-S bond distances vary from 2.1683(8) to 2.2114(8) Å, with a mean Mo-S bond length of 2.1872 Å (Table 5). Although the geometric parameters of **1** are in agreement with those in other thiomolybdates like $(enH_2)[MoS_4]$ (en = ethylenediamine) [26] or $[Co_2(tren)_3][MoS_4]_2$ [24], two of the Mo-S bond distances are longer,

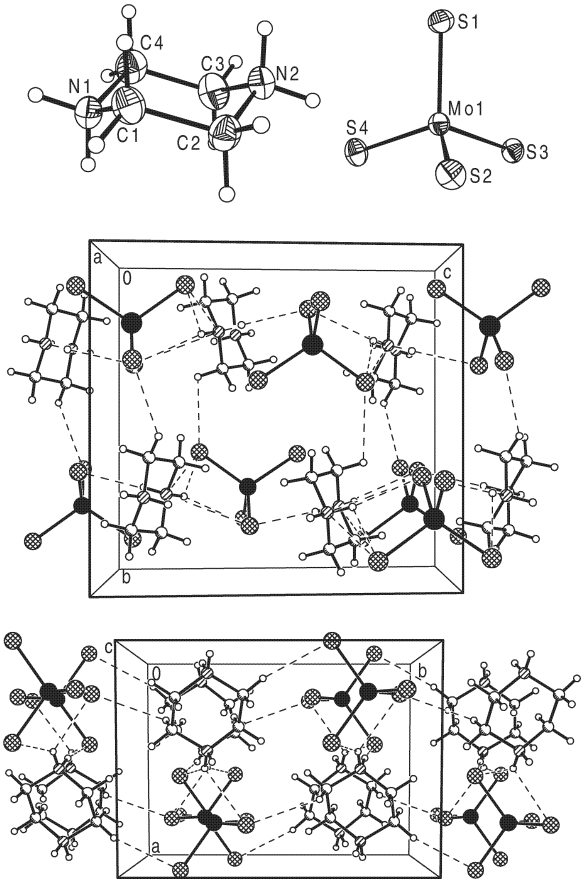

Fig. 1. Crystal structure of $(pipH_2)[MoS_4]$ **1** with labeling and displacement ellipsoids drawn at the 50% probability level (top), with view in the direction of the crystallographic *a*-axis (middle) and *c*-axis (bottom) (hydrogen bonding is shown as dashed lines).

while the other two distances are shorter than the average Mo-S bond length of 2.177(6) Å reported for $(Et_4N)_2[MoS_4]$ [21]. The elongation of Mo-S bond distances in **1** can be attributed to the observed short hydrogen bonding contacts (2.379 to 2.884 Å) between the cation and anion (Table 6). This results in an extended three-dimensional network as shown in Fig. 1. The S···H distances in **1** are shorter than the S···H distances of 2.55 to 3.02 Å reported for $(NH_4)_2[MoS_4]$ [20]. The atoms S(1,2,3) have two S···H contacts and S(4) has one such interaction. This feature is responsible for the very short Mo-S(4) distance of 2.1683 Å. The small D-H···A bond angle of 123.65° together with the longest S···H distance of 2.884 Å observed for S(4) indicates a very weak interaction. The shortest S···H distance of 2.379 Å is accompanied by the

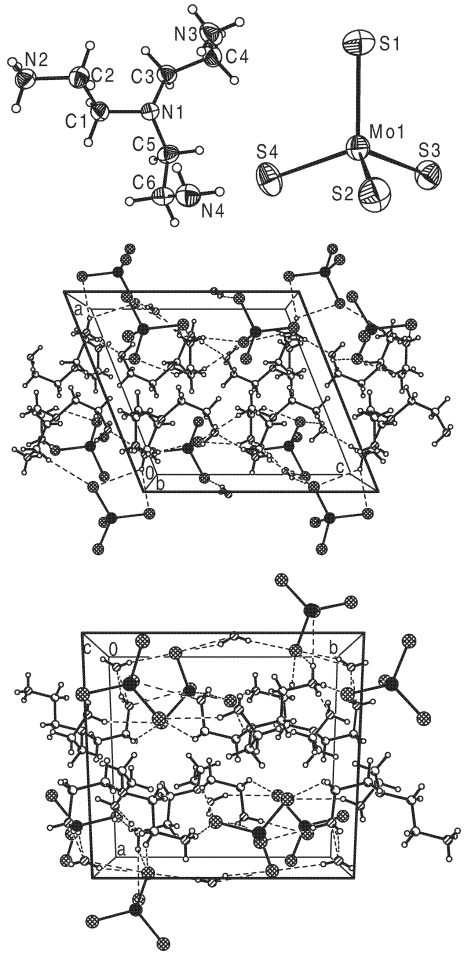

Fig. 2. Crystal structure of $(trenH_2)[MoS_4]\cdot H_2O$ **2** with labeling and displacement ellipsoids drawn at the 50% probability level (top), with view in the direction of the crystallographic *a*-axis (middle) and *c*-axis (bottom) (hydrogen bonding is shown as dashed lines).

largest D-H···A angle which can explain the long Mo-S(2) bond of 2.2114(8) Å. The intermediate Mo-S bond lengths can be similarly explained based on the strengths of the H-bonding interactions. To the best of our knowledge the Mo-S(2) distance of 2.2114(8) Å in **1** is one of the longest Mo-S bond lengths reported so far for tetrathiomolybdate complexes. It is also noted that the difference between the longest and the shortest Mo-S bond distances of 0.0431 Å in **1** is very large. This is probably responsible for the appearance of a split Mo-S vibration in the IR spectrum.

In the structure of **2** diprotonated tren cations, tetrathiomolybdate anions and crystal water are present (Fig. 2). Only two of the four N atoms in tren are protonated while the tertiary atom N(1) as well as one of the primary amino group N(4) are not protonated. A similar feature has been observed in $(trienH_2)[MoS_4]$ (trien = triethylenetetramine) which is derived from the isomeric amine trien [38]. All interatomic distances and angles in the tren cation are in agreement with the data reported for complexes containing the tren moiety like $[Co_2(tren)_3][MoS_4]_2$ [24]. As in **1** the $[MoS_4]$ tetrahedron is distorted with S-Mo-S angles between 107.89(2) and 110.97(2)° and Mo-S bond lengths from 2.1670(5) to 2.1951(5) Å, with a mean Mo-S distances of 2.1846 Å (Table 5). In **2** three of the Mo-S bonds are longer than the average Mo-S distance of 2.177 Å reported for $(Et_4N)_2[MoS_4]$ [21]. In **2** short S···H contacts are observed between the organic cation and the anion (Table 7), and the crystal water is also involved in two H···S(1) interactions. The resulting H bonding network is shown in Fig. 2. The S···H contacts range from 2.458 to 3.019 Å and are shorter than those (2.55 to 3.02 Å) reported for $(NH_4)_2[MoS_4]$ [20]. The shortest Mo-S bond length of 2.1670(5) Å is observed for S(3), which has only one contact to a H atom at a distance of 2.929 Å (Table 7). The analysis of the situation for S(1) and S(4) shows some interesting trends. The atom S(4) has two H atoms at distances 2.623 and 2.530 Å with corresponding angles of 153.12 and 169.34° and the longest Mo-S bond length of 2.1951(5) Å. On the other hand, S(1) has four interactions with H atoms, two with H atoms of the ammonium groups and two with H atoms of the water molecule. The two former are very weak (2.936 Å, angle: 120.06°; 3.019 Å, 128.29°) while the latter two interactions are significantly stronger (2.499 Å, 161.38°; 2.586 Å, 169.33°). The resulting Mo-S(1) bond of 2.1856(5) Å is surprisingly short as one would expect that this bond is at least as long as the Mo-S(4) bond. One possible explanation may be that despite the short S(1)···H distances to the H atoms of the water molecule the interactions are weaker than with H atoms bound to N with S···H separations of comparable lengths. Finally, S(2) has two short contacts (Table 7), and the Mo-S(2) bond amounts to 2.1905(5) Å. The difference between the longest and the shortest Mo-S bond distances in **2** of 0.0281 Å is slightly smaller than that observed in **1**.

In compound **3** three crystallographically independent $[(prop)_4N]^+$ cations are observed with two of them located in special positions (see Fig. 3). The C-C and C-N bond lengths as well as the angles observed

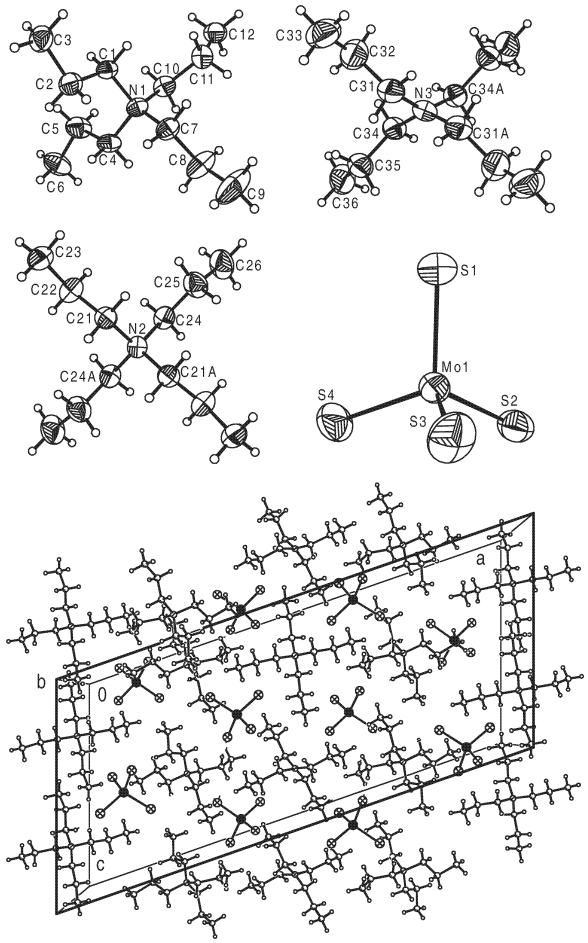

Fig. 3. Crystal structure of $[(prop)_4N]_2[MoS_4]$ **3** with labeling and displacement ellipsoids drawn at the 50% probability level (top), with view in the direction of the crystallographic *c*-axis (bottom).

for the cation are in the normal range. The S-Mo-S angles between 108.34(1)° and 110.25(1)° (Table 5) demonstrate the distortion of the $[MoS_4]^{2-}$ tetrahedron. The Mo-S bond lengths scatter in a more narrow range than in **1** and **2** with values from 2.1749(7) to 2.1928(7) Å and a mean Mo-S bond distance of 2.1850 Å. The difference between the longest and shortest bond amounts to 0.0179 Å and is the lowest value for all three compounds. It is interesting to note that the average Mo-S distance in **3** is significantly longer than in $(Et_4N)_2[MoS_4]$ of 2.177(6) Å.

Spectral studies

Several bands in the central part of the IR spectra observed for compounds **1**, **2** and **3** can be attributed to absorptions of the cations. The infrared spectrum of **2** exhibits a broad and strong band at around 3462 cm^{-1} that is assignable to the O-H stretching vibration of the crystal water. In contrast, the anhydrous compounds **1** or **3** are devoid of any bands above 3100 cm^{-1}. The N-H stretching vibrations appear at around 3000 cm^{-1} in **1** and at 3072 and 3004 cm^{-1} in **2**. Since complex **2** contains protonated amine as well as free amine more bands are observed for **2** in the N-H region. The shift to lower wave numbers compared to the free amine in **1** or **2** can be attributed to the H-bonding interactions (N-H···S) between the organic cation and the tetrathiomolybdate anion. For the free tetrahedral $[MoS_4]^{2-}$ anion four characteristic bands $\nu_1(A_1)$, $\nu_2(E)$, $\nu_3(F_2)$, and $\nu_4(F_2)$ are expected [16, 39]. All four bands are Raman active while only ν_3 and ν_4 are infrared active. Many tetrathiomolybdates exhibit a single strong band at around 475 cm^{-1} assignable to the triply degenerate asymmetric stretching vibration (ν_3) of the Mo=S bond [16, 26, 33]. Interestingly, for **1** this vibration is split up and appears as a doublet at 479 and 465 cm^{-1} with a further band around 445 cm^{-1}. The observed extra signals cannot be assigned to vibrations of the organic cation in view of the fact that no strong signals are observed for $(pipH_2)Cl_2$ below 500 cm^{-1}. Hence these features indicate considerable distortion of the $[MoS_4]$ tetrahedron and can be explained by the lowering in symmetry [16], which is probably responsible for the symmetric stretching vibration (ν_1) of the Mo=S bond at 445 cm^{-1} to appear as a medium intensity band. The IR inactive (ν_1) vibration is seldom observed for undistorted tetrahedral compounds. The assignment of the 445 cm^{-1} band for the symmetric stretching vibration gains credence form the observation of an intense signal in the Raman spectrum of **1** at 448 cm^{-1}. For **2** the IR absorptions are located at around 487 and 467 cm^{-1} with a very weak shoulder at 450 cm^{-1}. The same arguments can be used to explain the occurrence of three bands instead of one when the $[MoS_4]$ tetrahedron is not distorted. The reduced symmetry of the anion in **3** is also obvious from its IR spectrum. A broad asymmetric and intense band with the maximum located at 464 cm^{-1} is seen with a shoulder at 474 cm^{-1}. A third signal occurs at 448 cm^{-1}.

Thermal studies

The thermal stability of all three compounds was investigated using DTA-TG measurements. On heating

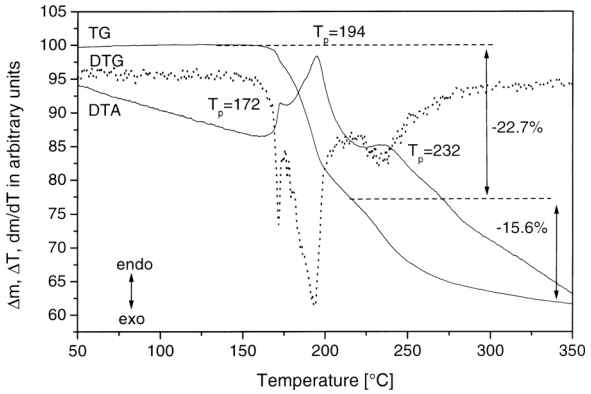

Fig. 4. DTA, TG and DTG curves for $(pipH_2)[MoS_4]$ **1** (heating rate 4 K/min; N_2 atmosphere; given are the peak temperatures (T_p) in °C and the mass loss in %).

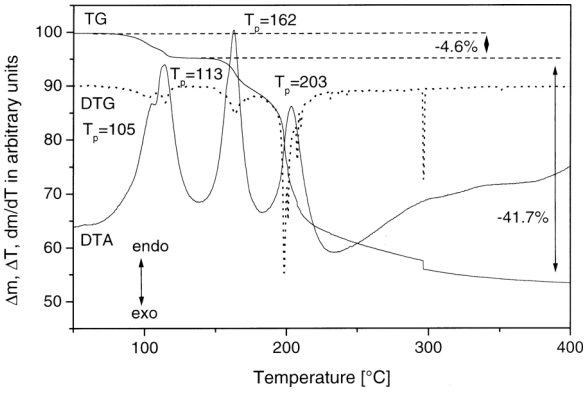

Fig. 5. DTA, TG and DTG curves for $(trenH_2)[MoS_4]\cdot H_2O$ **2** (heating rate 4 K/min; N_2 atmosphere; given are the peak temperatures (T_p) in °C and the mass loss in %).

compound **1**, the decomposition starts at about 170 °C, which is accompanied by endothermic events in the DTA at 172 and 194 °C (Fig. 4). From the DTG curve it is obvious that this reaction occurs in several steps, which cannot be fully resolved. The complete mass loss up to 330 °C where the DTG curve shows a minimum is about 38.3%, which is in good agreement with the emission of hydrogen sulfide and piperazine (Δm_{theo}(-piperazine/-H_2S) = 38.5%) resulting in the formation of MoS_3 according to the following equation (1):

$$(pipH_2)[MoS_4] \rightarrow pip + H_2S + MoS_3 \qquad (1)$$

The simultaneous emission of amine and H_2S has been observed by us earlier during a thermal decomposition study of $(1,3\text{-pn}H_2)[MoS_4]$ (1,3-pn is 1,3-propanediamine) [27]. On further heating of the sample, a slow mass decrease was observed and the residual mass of 60.6% at about 800 °C (not shown in the DTA-TG curve) shows that the intermediately formed MoS_3 is transformed into MoS_2. The elemental analysis of the black residue indicates that a small amount of C and N remained in the product, the X-ray powder pattern of which showed no sharp reflections but only broad humps indicating that an amorphous product was formed.

When compound **2** is heated a single mass step of 4.6% occurs at about 80 °C, which can be attributed to the loss of the water incorporated in the crystals (Δm_{theo}(-H_2O) = 4.6%) (Fig. 5). From the DTA and the DTG curve it is obvious that this reaction consists of two endothermic events, which occur at 105 and 113 °C. The loss of water is complete at about 140 °C. On further heating the sample mass decreases strongly and two endothermic events are observed at 162 and 203 °C. The DTG curve shows that the decomposition reaction proceeds in three different steps, which cannot fully be resolved. The experimental mass loss up to about 290 °C where the DTG curve shows a minimum is about 37.4% which is in good agreement with the loss of the amine ligands (Δm_{theo}(-tris(2-aminoethyl)amine)) = 37.4%). However, the C, H, N analysis of the final black residue revealed the presence of large amounts of organic matter and therefore, it can be assumed that as in the decomposition of compound **1** the amine and H_2S are emitted simultaneously. Upon a further increase of the temperature the sample mass decreases slowly. The C, H and N analytical data of the residue indicate the formation of a contaminated MoS_{3-x} sulfide. An X-ray examination of the residue showed it to be amorphous. Therefore, the decomposition of compound **2** follows predominantly the following equation (2):

$$(trenH_2)[MoS_4]\cdot H_2O \rightarrow tren + H_2S + MoS_3 + H_2O \qquad (2)$$

For **3**, DTA-TG measurements showed a strong endothermic event at 99 °C (Fig. 6). Because the sample mass remains constant it can be inferred that a phase transition occurs. With an increase in temperature, a mass loss is observed in two steps. The DTG curve shows that the first mass loss consists of several different successive steps, which cannot be fully resolved. The complete mass loss up to 360 °C is 69.6% which is slightly more than expected for the loss of the organic components and sulfur leading to the formation

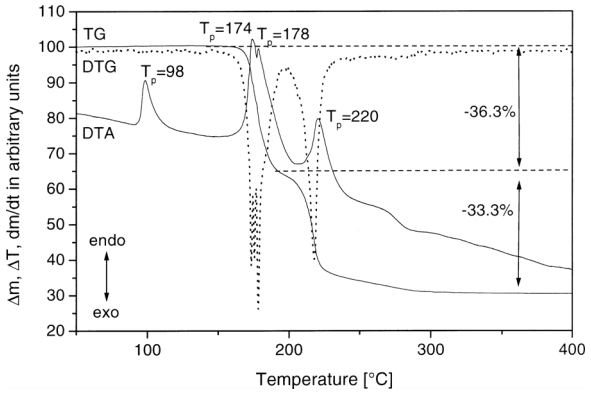

Fig. 6. DTA, TG and DTG curves for $[(prop)_4N]_2[MoS_4]$ **3** (heating rate 4 K/min; N_2 atmosphere; given are the peak temperatures (T_p) in °C and the mass loss in %).

of MoS_3 ($\Delta m_{theo}(-C_{24}H_{56}N_2S)$) = 67.8%). However, elemental analysis shows residual carbon in the product (composition: $MoS_2C_{0.7}$) suggesting that MoS_2 is formed.

The thermal properties of compound **3** were also investigated in the past [2, 40]. The authors proposed the following sequence of decomposition steps (3, 4):

$$\mathbf{3} \rightarrow (CH_3CH_2CH_2)_3N + CH_3CH_2CH_2NS + (CH_3CH_2CH_2)_4MoS_3 \quad (3)$$

$$(CH_3CH_2CH_2)_4MoS_3 \rightarrow (CH_3CH_2CH_2)_2S + CH_3(CH_2)_4CH_3 + MoS_2 \quad (4)$$

These reaction steps were obviously assigned based on the mass changes alone during the decomposition. In the earlier work an initial mass loss of 2% was also reported and attributed to elimination of impurities like trace amounts of water [40]. To shed further light onto this complex behavior we investigated the thermal reactions with DTA-TG measurements coupled with mass spectroscopy. In contrast to the previous investigations we find that the mass spectra in both steps are identical which show that in both steps the same compounds are emitted. An analysis of the pattern shows clearly that tripropylamine ($m/z =$ 143) is emitted in both steps. The remaining peaks can be assigned to the formation of dipropyldisulfide ($CH_3CH_2CH_2SSCH_2CH_2CH_3$; $m/z = 150$). There are no hints for the formation of $CH_3CH_2CH_2NS$, $(CH_3CH_2CH_2)_2S$ or $CH_3(CH_2)_4CH_3$ as proposed from the results obtained in previous investigations

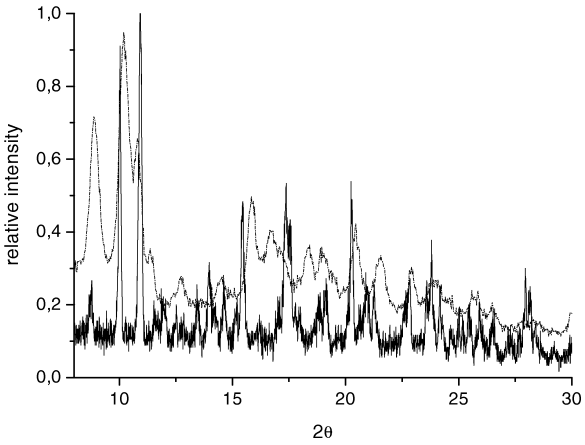

Fig. 7. X-ray powder pattern of compound **3** (full line) and of the product obtained when the thermal decomposition is stopped at 200 °C (dotted line).

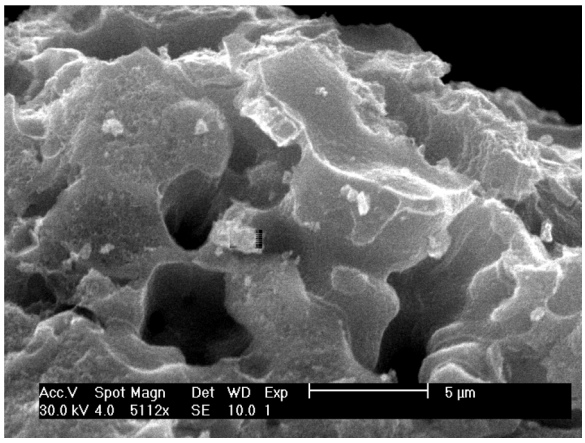

Fig. 8. SEM micrograph of the decomposition product of compound **3**.

[40]. The following equation may account for our observations (5):

$$\mathbf{3} \rightarrow 2\,(CH_3CH_2CH_2)_3N + (CH_3CH_2CH_2SSCH_2CH_2CH_3) + 2\,MoS_2 \quad (5)$$

However, if the reaction is stopped after the first TG step at about 200 °C, the X-ray powder pattern is completely different from that of the starting compound and does not correspond to that of MoS_3 or MoS_2 (Fig. 7). The relatively low modulation shows also that practically no amorphous molybdenum sulfides are present. This experiment is indicative of the fact that some unknown intermediate compound is formed and that the overall reaction must be more complicated.

The decomposition products were also examined with Scanning Electron Microscopy. The products of **1** and **2** are composed of fine particles with a plate-like morphology. In contrast the product of **3** shows pores with diameters in the μm range and a sponge-like morphology (Fig. 8). This observation is in accordance with literature results [2] where the mesoporosity was explained due to the accumulation of gases during the thermal decomposition process, the formation of channels being caused upon the escape of the gases to the surface of the material.

Acknowledgements

Financial support by the State of Schleswig-Holstein and the Deutsche Forschungsgemeinschaft (DFG) is gratefully acknowledged. Work done at Goa University is supported by the University Grants Commission (UGC) New Delhi under the Special Assistance Program.

[1] T. Rauchfuss, Inorg. Chem. **43**, 14 (2004) and references cited therein.
[2] G. Alonso, G. Berhault, A. Aguilar, V. Collins, C. Ornelas, S. Fuentes, R. R. Chianelli, J. Catal. **208**, 359 (2002).
[3] M. Breysse, E. Furimsky, S. Kasztelan, M. Lacroix, G. Perot, Catal. Rev. **44**, 651 (2002).
[4] D. D. Whitehurst, T. Isoda, I. Mochida, Adv. Catal. **42**, 345 (1988).
[5] F. Pedraza, S. Fuentes, Catal. Lett. **65**, 107 (2000).
[6] H. Nava, C. Ornelas, A. Aguilar, G. Berhault, S. Fuentes, G. Alonso, Catal. Lett. **86**, 257 (2003).
[7] D. Coucouvanis, Adv. Inorg. Chem. **45**, 1 (1998).
[8] E. D. Simhon, N. C. Baenziger, M. G. Kanatzidis, D. Coucouvanis, J. Am. Chem. Soc. **103**, 1218 (1981).
[9] W. H. Pan, M. A. Harmer, T. R. Halbert, E. I. Stiefel, J. Am. Chem. Soc. **106**, 459 (1984).
[10] M. Draganjac, E. Simhon, L. T. Chan, M. G. Kanatzidis, N. C. Baenziger, D. Coucouvanis, Inorg. Chem. **21**, 3321 (1982).
[11] S. A. Cohen, E. I. Stiefel Inorg. Chem. **24**, 4657 (1984).
[12] W. H. Pan, M. E. Leonowicz, E. I. Stiefel, Inorg. Chem. **22**, 672 (1983).
[13] G. J. Brewer, R. D. Dick, D. K. Grover, V. LeClaire, M. Tseng, M. Wicha, K. Pienta, B. D. Redman, T. Jahan, V. K. Sondak, M. Strawderman, G. Lecarpentier, S. D. Merajver, Clinical Cancer Res. **6**, 1 (2000).
[14] G. N. George, I. J. Pickering, H. H. Harris, J. Galler, D. Klein, J. Lichtmannegger, K. H. Summer, J. Am. Chem. Soc. **125**, 1704 (2003).
[15] J. J. Berzelius, Poggendorffs Ann. Phys. Chem. **7**, 262 (1826).
[16] A. Müller, E. Diemann, R. Jostes, H. Bögge, Angew. Chem. **93**, 957 (1981); Angew. Chem. Int. Ed. Engl. **20**, 934 (1981) and references therein.
[17] S. H. Laurie, Eur. J. Inorg. Chem. 2443, (2000).
[18] I. Bezverkhyy, P. Afanasiev, M. Lacroix, Inorg. Chem. **39**, 5416 (2000).
[19] I. Bezverkhyy, P. Afanasiev, M. Lacroix, Mater. Res. Bull. **37**, 161 (2002).
[20] D. E. Schwarz, T. B. Rauchfuss, S. R. Wilson, Inorg. Chem. **42**, 2410 (2003).
[21] M. G. Kanatzidis, D. Coucouvanis, Acta Crystallogr. **C39**, 835 (1983).
[22] J. Ellermeier, C. Näther, W. Bensch, Acta Crystallogr. **C55**, 501 (1999).
[23] J. Ellermeier, C. Näther, W. Bensch, Acta Crystayllogr. **C55**, 1748 (1999).
[24] J. Ellermeier, W. Bensch, Z. Naturforsch. **56b**, 611 (2001).
[25] J. Ellermeier, W. Bensch, Monatsh. Chem. **133**, 945 (2002).
[26] B. R. Srinivasan, B. K. Vernekar, K. Nagarajan, Indian J. Chem. **40A**, 563 (2001).
[27] B. R. Srinivasan, S. N. Dhuri, C. Näther, W. Bensch, Inorg. Chim. Acta, in press.
[28] B. R. Srinivasan, S. N. Dhuri, C. Näther, W. Bensch, Acta Crystallogr. **C59**, m124 (2003).
[29] B. R. Srinivasan, S. N. Dhuri, C. Näther, W. Bensch, Acta Crystallogr. **E58**, m622 (2002).
[30] B. R. Srinivasan, S. N. Dhuri, C. Näther, W. Bensch, Acta Crystallogr. **E59**, m681 (2003).
[31] J. Ellermeier, R. Stähler, W. Bensch, Acta Crystallogr. **C58**, m70 (2002).
[32] P. A. Koz'min, Z. V. Popova, Zh. Strukt. Khim. (Russ.) **12**, 99 (1971).
[33] J. W. McDonald, G. D. Friesen, L. D. Rosenhein, W. E. Newton, Inorg. Chim. Acta **72**, 205 (1983).
[34] G. M. Sheldrick, SHELXS-97: Program for the solution of crystal structures, University of Göttingen, Germany (1994).
[35] G. M. Sheldrick, SHELXL-97: Program for the refinement of crystal structures, University of Göttingen (1997).
[36] B. R. Srinivasan, C. Näther, W. Bensch, Acta Crystallogr. **E59**, m639 (2003).
[37] J. Tyrselova, L. Kuchta, F. Pavelcik, Acta Crystallogr. **C52**, 17 (1996).
[38] S. Pokhrel, K. S. Nagaraja, B. Varghese, J. Struc. Chem. **44**, 689 (2003).
[39] K. Nakamoto, Infrared and Raman Spectra of Inorganic and Coordination Compounds 4th Edition, John Wiley, New York (1986) 130.
[40] G. Alonso, G. Berhault, R. R. Chianelli, Inorg. Chim. Acta **316**, 105 (2001).